Journal of Molecular and Cellular Cardiology 91 (2016) 42–51

Contents lists available at ScienceDirect

Journal of Molecular and Cellular Cardiology

journal homepage: www.elsevier.com/locate/yjmcc

Original article

Novel insights on the relationship between T-tubular defects and contractile dysfunction in a mouse model of hypertrophic cardiomyopathy

C. Crocini [a], C. Ferrantini [b], M. Scardigli [a], R. Coppini [c], L. Mazzoni [c], E. Lazzeri [a], J.M. Pioner [b], B. Scellini [b], A. Guo [d], L.S. Song [d], P. Yan [e], L.M. Loew [e], J. Tardiff [f], C. Tesi [b], F. Vanzi [a], E. Cerbai [c], F.S. Pavone [a,g,h], L. Sacconi [a,h,*], C. Poggesi [b,**]

[a] European Laboratory for Non-Linear Spectroscopy, 50019 Florence, Italy
[b] Division of Physiology, Department of Experimental and Clinical Medicine, University of Florence, 50134 Florence, Italy
[c] Division of Pharmacology, Department "NeuroFarBa", University of Florence, 50139 Florence, Italy
[d] Division of Cardiovascular Medicine, Department of Internal Medicine and Francois M. Abboud Cardiovascular Research Center, Carver College of Medicine, University of Iowa, Iowa City, IA 52242, USA
[e] R. D. Berlin Center for Cell Analysis and Modeling, University of Connecticut Health Center, Farmington, CT 06030, USA
[f] Cellular and Molecular Medicine, University of Arizona, Tucson, AZ 85721, USA
[g] Department of Physics and Astronomy, University of Florence, 50019 Sesto Fiorentino, Italy
[h] National Institute of Optics, National Research Council, 50125 Florence, Italy

ARTICLE INFO

Article history:
Received 15 May 2015
Received in revised form 16 November 2015
Accepted 16 December 2015
Available online 20 December 2015

Keywords:
Hypertrophic cardiomyopathy
T-tubules
Excitation–contraction coupling
Imaging
Non-linear microscopy

ABSTRACT

Abnormalities of cardiomyocyte Ca^{2+} homeostasis and excitation–contraction (E–C) coupling are early events in the pathogenesis of hypertrophic cardiomyopathy (HCM) and concomitant determinants of the diastolic dysfunction and arrhythmias typical of the disease. T-tubule remodelling has been reported to occur in HCM but little is known about its role in the E–C coupling alterations of HCM. Here, the role of T-tubule remodelling in the electro-mechanical dysfunction associated to HCM is investigated in the Δ160E cTnT mouse model that expresses a clinically-relevant HCM mutation. Contractile function of intact ventricular trabeculae is assessed in Δ160E mice and wild-type siblings. As compared with wild-type, Δ160E trabeculae show prolonged kinetics of force development and relaxation, blunted force-frequency response with reduced active tension at high stimulation frequency, and increased occurrence of spontaneous contractions. Consistently, prolonged Ca^{2+} transient in terms of rise and duration are also observed in Δ160E trabeculae and isolated cardiomyocytes. Confocal imaging in cells isolated from Δ160E mice reveals significant, though modest, remodelling of T-tubular architecture. A two-photon random access microscope is employed to dissect the spatio-temporal relationship between T-tubular electrical activity and local Ca^{2+} release in isolated cardiomyocytes. In Δ160E cardiomyocytes, a significant number of T-tubules (>20%) fails to propagate action potentials, with consequent delay of local Ca^{2+} release. At variance with wild-type, we also observe significantly increased variability of local Ca^{2+} transient rise as well as higher Ca^{2+}-spark frequency. Although T-tubule structural remodelling in Δ160E myocytes is modest, T-tubule functional defects determine non-homogeneous Ca^{2+} release and delayed myofilament activation that significantly contribute to mechanical dysfunction.

© 2015 The Authors. Published by Elsevier Ltd. This is an open access article under the CC BY-NC-ND license (http://creativecommons.org/licenses/by-nc-nd/4.0/).

1. Introduction

The transverse-axial tubular system (TATS) [1] plays a fundamental role in cardiac function by allowing a fast propagation of action potentials (APs) throughout ventricular cardiomyocytes. As a consequence of the uniform electrical activation, synchronous Ca^{2+} release from the sarcoplasmic reticulum is guaranteed, ultimately inducing homogeneous myofilament activation and rapid contraction of the whole myocyte. As a proof of concept, acute disruption of TATS trough osmotic-shock promotes asynchronous Ca^{2+} release [2] and deteriorates mechanical function [3]. In cardiomyocytes from animal models

Abbreviations: TATS, Transverse-axial tubular system; AP, Action potential; E–C, Excitation–contraction; HF, Heart failure; HCM, Hypertrophic cardiomyopathy; cTnT, Cardiac troponin T; VSD, Voltage sensitive dye; AOD, Acousto-optic deflector; RAMP, Random access multi-photon; SS, Surface sarcolemma; TT, T-tubule; S/N, Signal-to-noise ratio; AP+, Electrically coupled T-tubules; AP−, Failing T-tubules; TTP, Time-to-peak; CaT50, Time of 50% Ca^{2+} decay.

* Correspondence to: L. Sacconi, National Institute of Optics (INO-CNR) c/o LENS, - European Laboratory for Non-linear Spectroscopy, Via Nello Carrara 1, 50019 Sesto Fiorentino (FI), Italy.
** Correspondence to: C. Poggesi, Department of Experimental and Clinical Medicine, Viale Morgagni 63, 50143 Florence, Italy.
E-mail addresses: sacconi@lens.unifi.it (L. Sacconi), corrado.poggesi@unifi.it (C. Poggesi).

http://dx.doi.org/10.1016/j.yjmcc.2015.12.013
0022-2828/© 2015 The Authors. Published by Elsevier Ltd. This is an open access article under the CC BY-NC-ND license (http://creativecommons.org/licenses/by-nc-nd/4.0/).

of cardiac diseases, local Ca^{2+} release is delayed both in areas where t-tubules are disrupted [4] and in close proximity to electrically uncoupled TATS elements [5,6]. Pathological alterations of the TATS have been identified using electron microscopy in human ventricular tissue from patients with cardiac hypertrophy or heart failure (HF) [7–10]. Comparing human specimens from patients with HF from different causes, i.e. post-ischemic HF, dilated cardiomyopathy and hypertrophic cardiomyopathy (HCM), Lyon et al. [11] found significantly lower T-tubule density in all failing human hearts, including end-stage HCM. However, little is known about T-tubular remodelling and function in early-stages of these cardiac diseases, particularly in HCM. HCM is a Mendelian heart disease characterized by left ventricular hypertrophy, which develops in the absence of other cardiac or extracardiac causes. Over 900 mutations in more than 20 genes have been so far identified as causes of HCM; most of these mutations involve components of the contractile machinery, establishing the paradigm that HCM is a sarcomeric disease [12]. Despite the fact that primitive alteration occurs at sarcomere level, secondary changes of intracellular Ca^{2+} handling have also been reported in HCM patients as major contributors of diastolic dysfunction Peculiar histological features of HCM myocardium are prominent interstitial fibrosis and cardiomyocytes disarray [13] accompanied by ultrastructural changes, such as myofilament disarray, which may go hand in hand with changes of T-tubular architecture [14] and arrhythmogenic hazard in this disease [15].

In a subset of patients, HCM is associated with cardiac troponin T (cTnT) mutations in the form of missense, deletion, or splicing site mutations [16]. Deletion of the codon for a glutamic acid at position 160 of the protein (cTnT Δ160E) is associated with high risk of sudden cardiac death in patients [17,18]. Transgenic mice expressing Δ160E cTnT at 35% of total cTnT exhibit both mutation-driven changes in myofilament function (increased Ca^{2+}-sensitivity and increased energy cost of tension generation due to altered cross bridge kinetics [19]) and secondary Ca^{2+} handling alterations of cardiomyocytes (e.g. prolonged global Ca^{2+} transients) [20]. The cTnT Δ160E mouse model represents a well-suited candidate to study the functional impact of T-tubular remodelling in early-stage HCM, focusing on the interplay between mechanical alterations and changes of local Ca^{2+} release related to T-tubule anomalies.

2. Materials and methods

2.1. Animals

Twenty-four to 32 week old C57Bl/6 knock-in mice expressing a c-myc-tagged human cTnT with a heterozygous deletion of Glu160 (Δ160E) are used. The transgenic line is generated with a transgene expression level at 35% of total cTnT. The line is backcrossed to C57Bl/6 wild-type (WT) mice for 8–10 generations and protein expression verified at each generation. Each animal is genotyped via PCR-amplified tail DNA. Sibling mice are used to provide non-transgenic controls.

2.2. Trabeculae dissection

Right ventricular trabeculae are dissected from non-transgenic and cTnT Δ160E mouse hearts as previously described [21]. Briefly, the heart is excised and the proximal aorta is perfused retrogradely with a modified Krebs–Henseleit (KH) solution. KH solution contained (mM): 120 NaCl, 15 KCl, 2 $MgSO_4$, 1.2 NaH_2PO_4, 20 $NaHCO_3$, 0.50 $CaCl_2$, and 10 glucose, 20 butanedione-monoxime (BDM), pH 7.4 equilibrated with 95% O_2/5% CO_2. Thin (50–200-μm diameter) unbranched uniform trabeculae, running between the free wall of the right ventricle and the atrioventricular ring, are selected and carefully dissected.

2.3. Force measurements

Isometric twitch tension is measured from intact trabeculae as previously described [3,21]. Ventricular trabeculae are mounted between the basket-shaped platinum end of a force transducer (KG7A; Scientific Instruments) and a motor (Aurora Scientific Inc.), connected to micromanipulators. Muscles are initially perfused with the KH solution without BDM and 5 mM KCl at room temperature and stimulated at 0.5 Hz. Subsequently, baseline conditions are set (1 Hz, 30 °C, 2 mmol/l [$CaCl_2$]). Muscles are allowed to stabilize for at least 20–30 min before the experimental protocol begins. In a subset of experiments, force measurements are combined with intracellular calcium measurements.

2.4. Evaluation of protein expression level

Myofibril isolation and subsequent protein electrophoresis analysis of α- and β-myosin heavy chain (MHC) expression levels are performed as described previously [22–24] Briefly, the MHC isoform composition of mouse cardiac samples is assessed using a minigel electrophoresis system and a non-gradient gel by a procedure derived from Talmadge & Roy, 1993 [25]. Electrophoresis is carried out at 4 °C for 19 h at 70 V. The appropriate gel thickness (1 mm instead of 0.75 mm, in order to reduce resistance) combined with low glycerol concentration in the separating gel, low voltage and prolonged running time allowed us to achieve the resolution required for the separation of the two adult cardiac MHC isoforms. Gels are stained with Coomassie Blue for quantitative analysis. The stained gels are digitalized and analysed with a specific software (UN-SCAN-IT gel 6.0 software (Silk Scientific, Inc., UT, USA), allowing quantification of band intensity. Each band (α- or β-MHC) is expressed as percentage of the total MHC.

2.5. Cardiomyocytes isolation and Ca^{2+} re-adaptation

Ventricular cardiomyocytes are isolated by enzymatic dissociation. Isolation of single myocardial cells from C57Bl/6 (transgenic or not) is performed as described before [6]. Briefly, the animal is heparinized (5000 U/kg, i.p.) and deeply anaesthetised with Isoflurane. The excised heart is immediately bathed in cell isolation buffer and the proximal aorta is cannulated for retrograde perfusion. Buffer solution contains (in mM): 113 NaCl, 4.7 KCl, 0.6 KH_2PO_4, 0.6 Na_2HPO_4, 1.2 $MgSO_4$–$7H_2O$, 12 $NaHCO_3$, 10 $KHCO_3$, 10 Hepes, 30 taurine, 10 glucose, 10 2,3-butanedione monoxime, pH 7.3 (adjusted with NaOH). The coronary arteries are perfused with the same buffer solution at 37 °C for 3–4 min at a constant flow of 2–3 ml/min. The solution is then switched to a recirculating enzyme solution made of the same buffer supplemented with 0.1 mg/ml Liberase TM (Roche Applied Sciences). After 7–8 min, the ventricles are excised and cut into small pieces in buffer solution supplemented with 1 mg/mL bovine serum albumin. Gentle stirring facilitates further dissociation of myocytes. The cell suspension is let to settle and the cell pellet is resuspended in Tyrode buffer (in mM): 113 NaCl, 4.7 KCl, 1.2 $MgCl_2$, 10 glucose, and 10 HEPES; pH adjusted to 7.35 with NaOH supplemented with 10 μM blebbistatin and 4 μM cytochalasin D. Cells are gradually readapted to calcium, adding steps of 50 or 100 μM $CaCl_2$ every 5–8 min, until a concentration of 500 μM $CaCl_2$ is reached. Cells are loaded in extracellular buffer added with 10 μM blebbistatin, 4 μM cytochalasin D, and 500 μM $CaCl_2$.

2.6. Measurements of global intracellular Ca^{2+} transient in intact trabeculae and single cells

Intracellular calcium was measured from intact trabeculae as previously described [3]. The muscles are loaded with the cell-permeant acetoxymethyl ester form of the fluorescent intracellular Ca^{2+} indicator fura 2-AM (Life Technologies). In details, dissected trabeculae are

incubated for 30 min at 37 °C with a modified KH solution (containing, in mM: 120 NaCl, 5 KCl, 2 $MgSO_4$, 1.2 NaH_2PO_4, 20 $NaHCO_3$, 1 $CaCl_2$, 10 glucose, 10 HEPES, pH 7.35 adjusted with NaOH) added with 10 μM fura 2-AM, 10 μM (−)-blebbistatin and 10 μl/ml PowerLoad™ Concentrate, 100× (Life Technologies). After 30 min, loaded trabeculae are washed with the same KH solution, free of fura 2-AM and PowerLoad™ Concentrate (but still containing 10 μM blebbistatin and 1 mM $CaCl_2$); loaded trabeculae are then left at room temperature for 10–15 min to allow fura 2-AM de-esterification and finally mounted isometrically and field stimulated to record intracellular Ca^{2+} transients.

Intracellular calcium is measured from single cardiomyocytes as previously described [15]. Myocytes are incubated 30 min with the Ca^{2+} indicator Fluoforte (Enzo Life Sciences) at room temperature, washed and transferred to a temperature-controlled recording chamber (experimental temperature = 35 ± 0.5 °C), mounted on the stage of an inverted microscope. The SR Ca^{2+} load is quantified by rapid exposure to caffeine (20 mM), as previously described [15]. Briefly, timing of caffeine exposure is adjusted in order to reproduce the cycle-length of baseline stimulation. SR Ca^{2+} content is evaluated from the amplitude of caffeine-induced Ca^{2+} transients.

2.7. Cardiomyocytes labelling and confocal imaging

For T-tubules architecture analysis, cardiomyocytes are stained by adding to the cell suspension 2 μg/mL of the voltage sensitive dye (VSD) di-4-AN(F)EPPTEA [26] (dissolved in ethanol). After washing, cells are resuspended in fresh Ca^{2+} free solution containing 10 μM blebbistatin, 4 μM cytochalasin D. Loaded preparations are used for experiments within 30 min. The staining and imaging sessions are performed at room temperature (20 °C). For immunohistochemistry, cells are fixed with 4% paraformaldehyde in phosphate buffered saline (PBS) for 30 min. Cells are then washed in PBS added with 1% of bovine serum albumin (BSA) three times for 15 min. Cells are permeabilized with 0.1% Triton X-100 in PBS for 6 min and rinsed three times with fresh PBS. Cells are then treated with blocking solution (3% BSA in PBS) for 30 min and washed twice with PBS. Primary antibodies are incubated overnight at 4 °C: polyclonal anti-caveolin 3 (ab2912: Abcam) at 1:20 dilution in PBS and monoclonal anti-alpha-actinin (A7811; Sigma-Aldrich) at 1:800 dilution in PBS. After washing, secondary antibody is incubated for three hours: AlexaFluor488 donkey anti-mouse (ab150105; Abcam) at 1:250 dilution in PBS and AlexaFluor594 goat anti-rabbit (ab150092; Abcam) at 1:20 dilution. Confocal imaging is performed with a Nikon Eclipse TE300, with the Nikon C2 scanning head and with the Nikon Plan EPO 60× objective (numerical aperture 1.4, oil-immersion). Excitation laser at 488 nm is used for VSD and AlexaFluor488 and 561 nm for AlexaFluor 594.

2.8. T-tubules detection and analysis

Quantitative analysis of the T-tubule system is obtained by employing AutoTT, an automated T-tubule analysis algorithm [27], to confocal images. This approach prevents flaws due to the fact that density of T-tubules as well as non-T-tubule signals in the images influence the power spectrum generated by FFT. The global T-tubular architecture is skeletonized by AutoTT to extract the morphological patterns and to discriminate transverse and axial elements of the system. The densities of transverse and axial elements are determined by dividing the total pixels of each T-tubular component by the intracellular area of the region of interest. To analyse the regularity of the overall/global T-tubule system, AutoTT applies a 2-D FFT to the skeletonized global T-tubule image and calculates the power spectrum in the spatial frequency domain. A 2-D peak detection program is used to automatically detect the magnitude of the direct current (DC) component and the major (1st harmonic) frequency. The program automatically calculates the regularity of the TATS, defined as the magnitude of the major frequency normalized to that of the DC component.

2.9. RAMP microscope and simultaneous multisite recording of electrical activity and local Ca^{2+} release

Cardiomyocytes staining for random access multi-photon (RAMP) microscopy is performed by incubating the suspension for 15 min in 0.5 μg/ml of the Ca^{2+} indicator GFP-Certified™ FluoForte™ (Enzo Life Science). The dye is diluted in 1.5 ml buffer to the indicated concentration from a stock dissolved in DMSO. After washing, the cells are incubated with 2 μg/mL of the voltage sensitive dye (VSD) di-4-AN(F)EPPTEA [26] (diluted in 1.5 buffer from a stock dissolved in ethanol). Finally, the cells are resuspended in fresh extracellular buffer containing 10 μM blebbistatin, 4 μM cytochalasin D and 1 mM $CaCl_2$. Loaded preparations are used for experiments within 30 min. The staining and imaging sessions are performed at room temperature (20 °C). The RAMP imaging system has been already described [5,6]. In brief, a 1064 nm fibre laser provides the excitation light. The scanning head of the apparatus is provided by two orthogonally-oriented acousto-optic deflectors (AODs) and then the excitation light is focused onto the specimen by the objective lens. The two-photon fluorescence signal is collected forward and backward by an oil immersion condenser and the objective, respectively. The voltage and Ca^{2+} signals are discriminated by using a dichroic mirror beamsplitter at 605 nm. The fluorescence signals are detected by two independent photomultiplier tubes (H7422, Hamamatsu). Emission filters of 655 ± 20 nm and 520 ± 16 nm are used for voltage and Ca^{2+} detection, respectively. The large Stokes shift of fluorinated VSD is not sufficient to prevent spectral contamination between the two channels. A simple un-mixing procedure is thus used as previously reported [5]. The measurements are performed during steady-state stimulation (0.34 Hz). The cells are field-stimulated using two parallel platinum wires (250 μm in diameter) placed at a distance of 6.3 mm. Square pulses of 10–20 V and duration of 3 ms are used to reach AP threshold. In a typical measurement, we probe 5–10 different sarcolemmal sites for ten subsequent trials. The length of the scanned lines ranges from 2 to 10 μm with an integration time per membrane pass of ~200 μs, leading to a temporal resolution of 0.4–2 ms. The high spatio-temporal resolution of RAMP microscopy allows to assess the kinetic properties of local Ca^{2+} rise in close proximity to the T-tubules. Conversely, the scanning modality (focused on T-tubule sarcolemma) and the experimental condition employed for RAMP microscopy in this study (presence of the E–C uncoupler blebbistatin 1 μM, low stimulation frequency, 1 mM extracellular Ca^{2+}, low temperature) are not optimized for studying other features of local intracellular Ca^{2+} handling, e.g. Ca^{2+} reuptake.

2.10. Statistical analyses

Data are expressed and plotted as means ± SEM (Standard Error of Mean) obtained from a number of independent determinations on different myocytes or trabeculae. Number of cells/trabeculae (n) and number of animals (N) are indicated in the figure legends for each set of measurements. Unpaired Student's t-test is used for comparisons. A p-value of <0.05 is considered statistically significant ($^*p < 0.05$, $^{**}p < 0.01$, $^{***}p < 0.001$). All measurements aiming at comparing WT to cTnT Δ160E are based on the following assumptions: i) the variance of different preparations derived from single animals is comparable with the variance found among different animals; ii) the number of preparations derived from each animal is comparable. In measurements performed with RAMP microscopy on cTnT Δ160E cardiomyocytes, we also compare the behaviour of single subcellular elements, i.e. AP+ and AP− tubules and therefore the statistical n is the number of T-tubules.

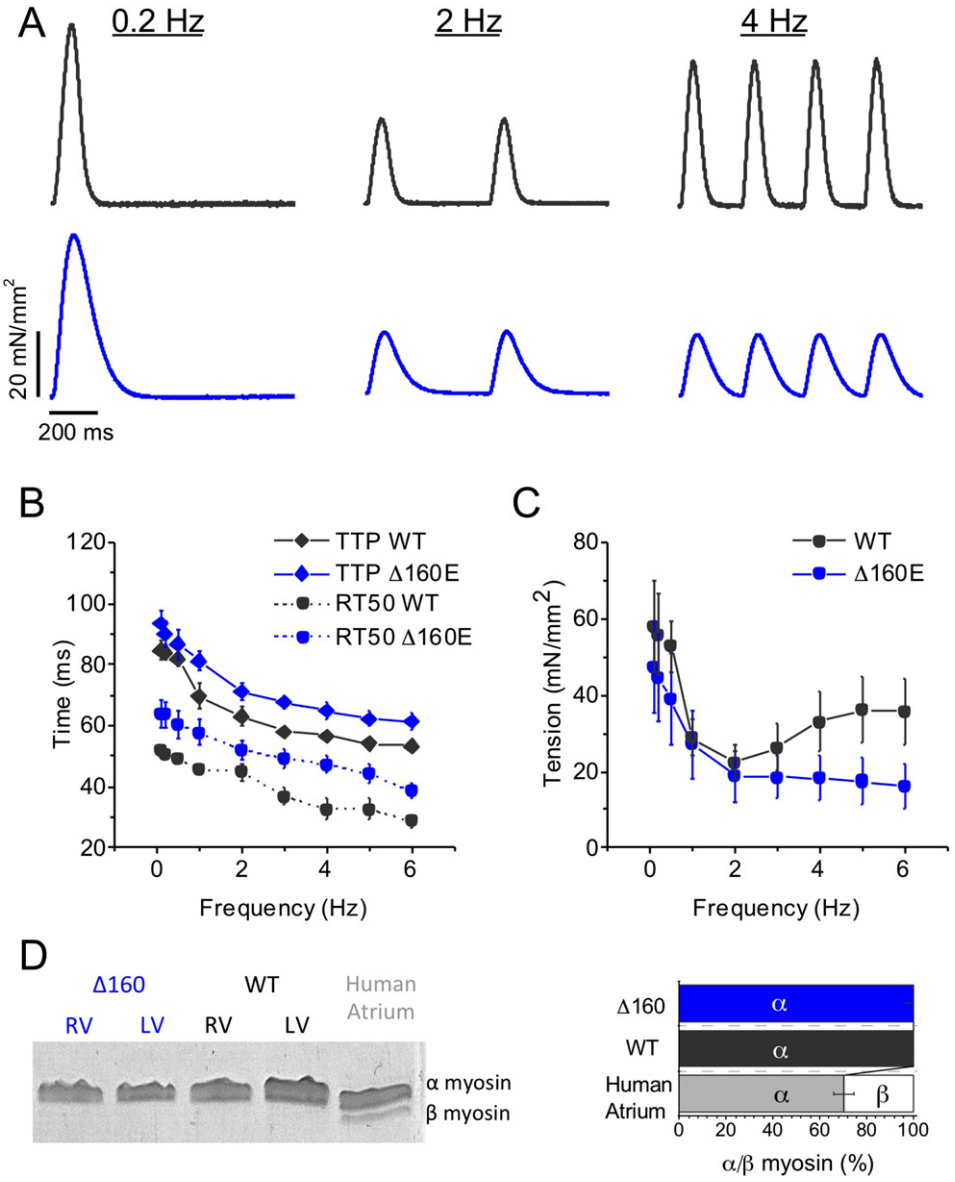

Fig. 1. Steady-state interval-force relationship. (A) Representative twitch traces from WT (grey) and cTnT Δ160E (blue) ventricular trabeculae recorded at 0.2, 2 and 4 Hz stimulation frequencies. cTnT Δ160E trabeculae show prolonged contraction at every stimulation frequency when compared to WT. At 4 Hz, cTnT Δ160E trabeculae also show a reduced twitch tension amplitude compared to WT. (B) Curves showing time from stimulus to peak contraction (TTP, solid line) and time from peak to 50% relaxation (RT50, dashed line) in WT (grey) and cTnT Δ160E (blue) trabeculae. (C) Data depicting frequency-dependence of twitch amplitude in WT (grey) and cTnT Δ160E (blue) trabeculae. Data reported as mean ± SEM calculated from 16 WT trabeculae and 15 cTnT Δ160E (N = 12 WT and 10 cTnT Δ160E). (D) Representative 8% SDS-PAGE gel of myofibril suspensions from left and right ventricles of Δ160E and WT hearts. Control human atrial myofibrils are used for comparison to identify the position of the β-myosin band; only α-MHC is expressed in Δ160E and WT hearts. On the right, a quantification in percentage is reported (N = 5 WT, N = 4 cTnT Δ160E).

3. Results

3.1. Steady-state interval-force relationship in cTnT Δ160E trabeculae

In the current study, force is measured from isometrically mounted mouse ventricular trabeculae stimulated at frequencies from 0.1 to 6 Hz at optimum myofilament overlap (sarcomere length 2.15 ± 0.05 μm). Trabeculae of cTnT Δ160E mice show prolonged steady-state twitch duration, with slower kinetics of both force generation and relaxation (Fig. 1A–B). Despite similar twitch tension at low stimulation frequencies (<1 Hz), cTnT Δ160E trabeculae show impaired positive inotropic response to high pacing rate (Fig. 1C). In fact, force-frequency curves of WT and cTnT Δ160E trabeculae start to diverge at 2 Hz, depicting the inability of mutant myocardium to respond properly to higher stimulation frequencies. We found that the prolonged and blunted twitch tension is not associated with α- to β-MHC isoform shift: cTnT Δ160E expresses exclusively the α-MHC isoform (Fig. 1D).

3.2. Short-term interval-force relationship in cTnT Δ160E trabeculae

A mechanical restitution protocol is used to evaluate the recovery properties of the E–C coupling machinery. Fig. 2A shows two representative traces recorded from WT and cTnT Δ160E trabeculae, the latter displaying increased amplitude of the premature extrasystolic beat. In Fig. 2B the amplitude of the premature beat (400 ms interval) is quantified as a percentage of steady state 1 Hz twitches. The mean amplitude of the extrasystolic beat is increased in cTnT Δ160E, indicating shorter sarcoplasmic reticulum (SR) refractoriness. We also test the enhancement of twitch tension in response to stimulation pauses (post-rest potentiation), reflecting the ability of the SR to accumulate Ca^{2+}.

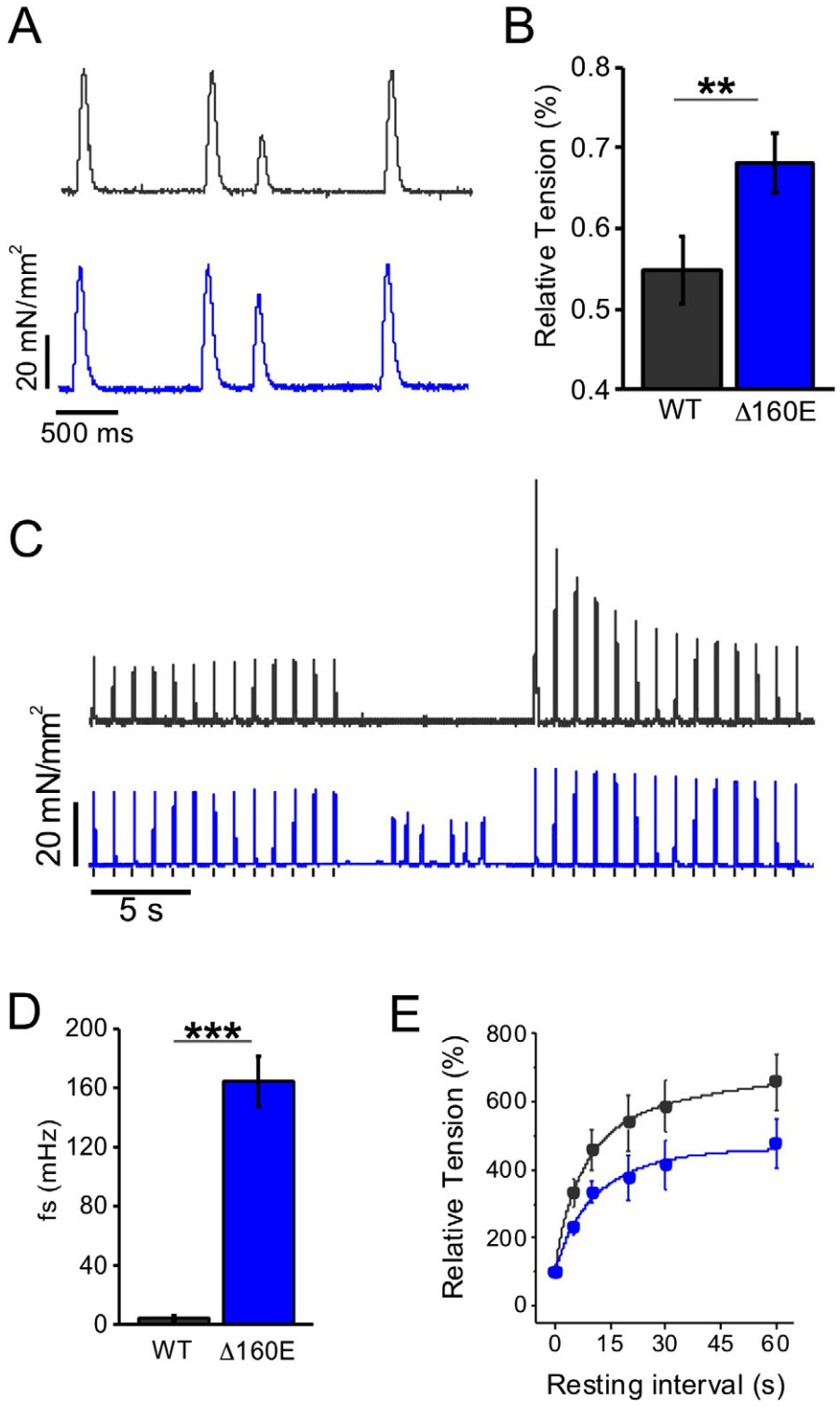

Fig. 2. Short-term interval force relationship. (A) Examples of premature contractions in WT (grey) and cTnT Δ160E ventricular trabeculae (blue). An extra-stimulus at 400 ms is inserted into a sequence of steady-state stimuli at 1 Hz. The tension amplitude in the cTnT Δ160E trabecula is increased compared to the WT. (B) The amplitude of the premature contraction is quantified as a percentage of steady state 1 Hz twitches. Data reported as mean ± SEM calculated from 12 WT trabeculae and 10 cTnT Δ160E (N = 9 WT and 8 cTnT Δ160E). (C) Representative traces of post-rest potentiation protocols in WT (grey) and cTnT Δ160E (blue) ventricular trabeculae. In the experiments, resting intervals vary from 5 to 60 s. Here, representative traces for pauses of 10 s are reported. The cTnT Δ160E trabecula shows spontaneous contractions during the stimulation pause. (D) Frequency of spontaneous contractions during stimulation pauses. (E) Amplitude of post rest contractions (relative to 1 Hz twitches) at different resting intervals. Data calculated from 15 WT trabeculae and 10 cTnT Δ160E (N = 11 WT and 8 cTnT Δ160E). Students's t-test $^{**}p < 0.01$ and $^{***}p < 0.001$.

Stimulation pauses vary from 5 to 60 s and are inserted into a steady-state 1-Hz series (Fig. 2C). The frequency of spontaneous contractile events occurring during pauses in cTnT Δ160E and WT is quantified (Fig. 2D). WT trabeculae never exhibit spontaneous activity during stimulation pauses, while cTnT Δ160E trabeculae frequently do. The presence of spontaneous activity during pauses is accompanied by

depressed post-rest potentiation of force, as reported in Fig. 2E. These results suggest an increased disposition of the transgenic myocardium to uncontrolled Ca^{2+} release and Ca^{2+} leakage from the SR.

3.3. Global Ca^{2+} transient in cTnT Δ160E trabeculae and isolated cardiomyocytes

The slower kinetics of both force generation and relaxation are associated with prolonged duration of global Ca^{2+} transient in cTnT Δ160E trabeculae in terms of time to peak and decay (Fig. 3A). To clarify the cellular basis of the kinetic changes revealed in multicellular preparations, we study intracellular Ca^{2+} fluxes in isolated cardiomyocytes. Indeed, we found that kinetics of both Ca^{2+} transient rise and decay (Fig. 3B) are slower in cTnT Δ160E cardiomyocytes compared to WT, in line with our data on intact trabeculae and previous findings on single cells [28]. Notably, the decay of caffeine-induced Ca^{2+} transient is slower in cTnT Δ160E cardiomyocytes, suggesting reduced NCX activity.

We also observed that cTnT Δ160E cardiomyocytes show significantly reduced Ca^{2+} transient amplitude at high stimulation frequency (5 Hz), despite a preserved amplitude at 1 Hz (Fig. 3B). Diastolic Ca^{2+} levels are higher in cTnT Δ160E (Fig. 3B) and SR Ca^{2+} load, assessed during steady-state stimulation, is reduced (Fig. 3C).

3.4. T-tubular and sarcomeric architecture explored by confocal imaging

The Ca^{2+} transient alterations (i.e. the slower Ca^{2+} rise) found in cTnT Δ160E preparations prompted us to examine the topology of the TATS in this model. Living isolated cardiomyocytes labelled with di-4-AN(F)EPPTEA are studied by confocal imaging. In Fig. 4A, two representative confocal images of WT and cTnT Δ160E cardiomyocytes are reported. Images are then analysed with a software for automatic detection and analysis of T-tubular architecture (Auto-TT [27]). On average, we find a mild remodelling of TATS in cTnT Δ160E compared to WT cardiomyocytes. As shown in Fig. 4A, a significant but small reduction of transverse elements and architecture regularity is observed. The amount of axial elements is not changed in diseased cardiomyocytes.

Considering the prominent ultrastructural disarray found in cTnT Δ160E cardiomyocytes [20], the juxtaposition between T-tubules and Z-lines is assessed here by immunohistochemistry. A cross correlation analysis between T-tubules (red in Fig. 4B) and Z-lines (green in Fig. 4B) fluorescence signal is performed in WT and in cTnT Δ160E cells. We find a Pearson product–moment correlation coefficient of 0.69 ± 0.01 and 0.71 ± 0.01 in WT and cTnT Δ160E, respectively (data reported as mean ± SEM calculated from 26 WT and 23 cTnT Δ160E cells). No statistically significant difference (Students's t-test $p = 0.09$) is found between the two groups. The lack of massive structural alterations at T-tubular and sarcomeric level drove us to evaluate potential electrical defects of TATS.

3.5. Kinetics of Ca^{2+} release in cTnT Δ160E isolated cardiomyocytes

Functional properties of the E–C coupling machinery are here assessed by using RAMP microscopy, which is capable to dissect the spatio-temporal relationship between T-tubular electrical activity and the correspondent local Ca^{2+} release at multiple sites within the same cardiomyocyte [5,6]. Isolated WT and cTnT Δ160E cardiomyocytes are stained with di-4-AN(F)EPPTEA and GFP-certified FluoForte (Fig. 5A). The figure shows a specific and homogeneous labelling of the

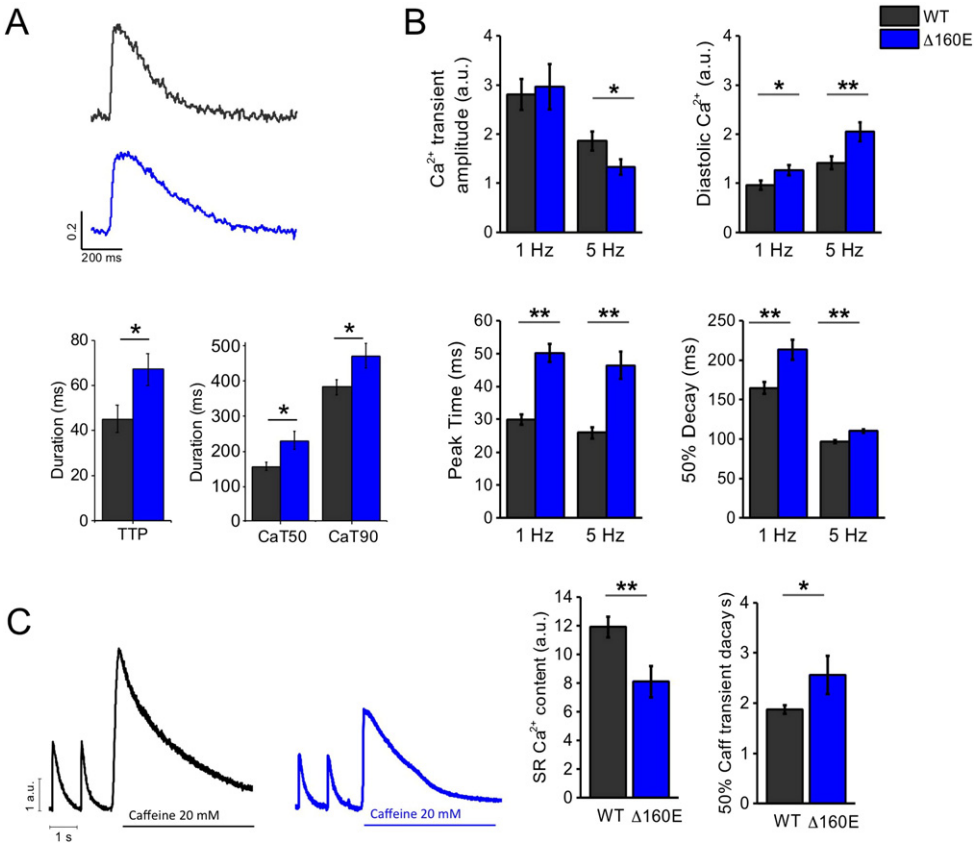

Fig. 3. Global calcium transients in cTnT Δ160E trabeculae and cardiomyocytes. (A) Representative global Ca^{2+} transients recorded from WT (grey) and cTnT Δ160E (blue) trabeculae, labelled with Fura-2 AM. In the panel below, time to peak (TTP), 50% (CaT50), and 90% (CaT90) decay of Ca^{2+} transients recorded in ventricular trabeculae (n = 6 from N = 3 WT and n = 5 from N = 3 cTnT Δ160E mice3 cTnT Δ160E mice). (B) Amplitude of Ca^{2+} transients and diastolic Ca^{2+} levels recorded in WT and cTnT Δ160E cells at 1 and 5 Hz. Below, graphs depicting the duration of Ca^{2+} transients at 1 and 5 Hz. (C) Representative examples of SR Ca^{2+} load assessed during rapid application of caffeine 20 mM and calculated from the amplitude of caffeine-induced Ca^{2+} transients at 1 Hz in WT and Δ160E cardiomyocytes (n = 49 cells of N = 5 WT and n = 37 cells of N = 4 cTnT Δ160E mice). Students's t-test *p < 0.05 and **p < 0.01.

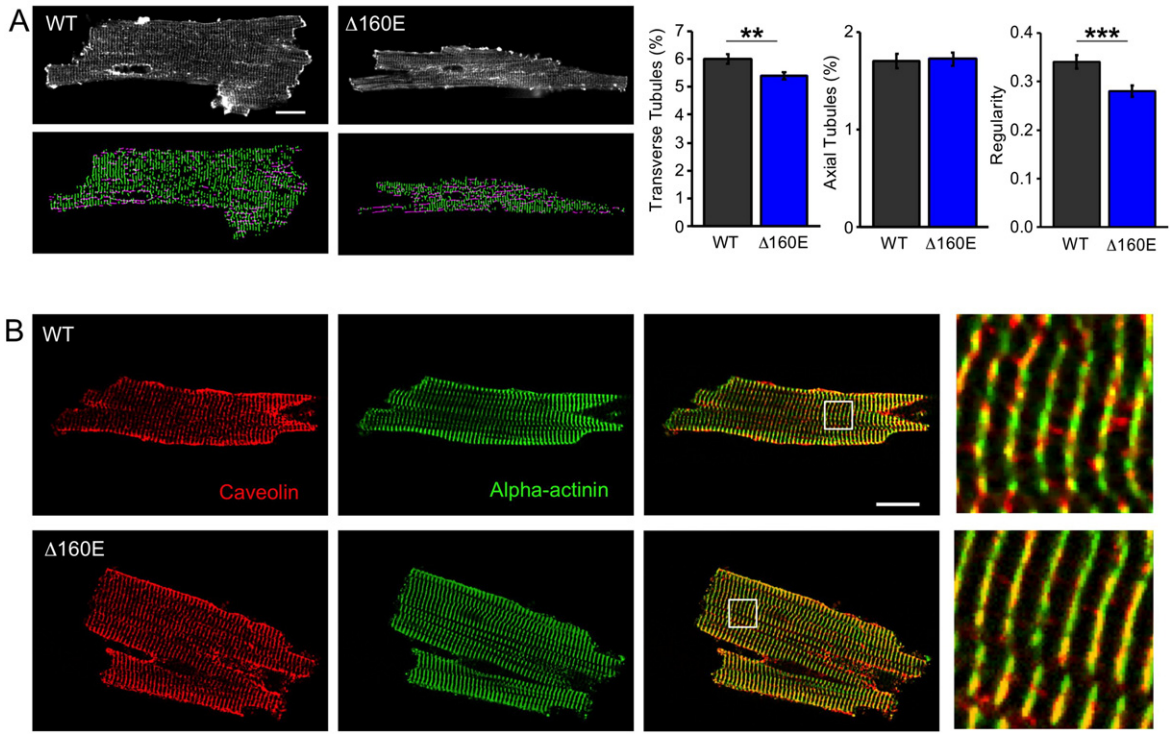

Fig. 4. TATS architecture and sarcomeric alignment. (A) Two representative confocal images of WT and cTnT Δ160E cardiomyocytes. Sarcolemma stained with di-4-AN(F)EPPTEA. In the bottom panels, correspondent images of same cells showing skeletonized T-tubular system, obtained with AUTO-TT. Transverse elements are shown in green and axial ones in magenta. On the right, columns showing the density of transverse and axial tubules, as well as TATS regularity in WT and cTnT Δ160E cardiomyocytes. Data reported as mean ± SEM calculated from 39 WT cells and 46 cTnT Δ160E. Students's t-test $^{**}p < 0.01$ and $^{***}p < 0.001$. (B) Immunofluorescence analysis of sarcomeres and T-tubules in WT and cTnT Δ160E isolated cardiomyocytes. Cells are stained with anti-caveolin-3 (red) and anti-α-actinin (green) primary antibodies for labelling TATS and z-lines, respectively. The white inset is magnified in the right panel. Scale bars: 20 μm.

sarcolemma by the VSD (magenta), whereas FluoForte (green) is present uniformly in the whole cell. The RAMP microscope is used to simultaneously probe both changes in membrane potential and $[Ca^{2+}]_i$ at different sites by scanning multiple non-contiguous sarcolemmal regions. Examples of simultaneous optical recording from three different membrane sites (surface sarcolemma, SS and two different T-tubules, TTi) are reported for WT and cTnT Δ160E in Fig. 5A. The signal-to-noise ratio (S/N) is sufficient to detect the presence of an AP occurring on the probed sarcolemma regions and to assess the temporal features of Ca^{2+} rise in the surrounding cytoplasm. In cTnT Δ160E myocytes, we observe (23 ± 5)% of T-tubules failing to propagate AP (Fig. 5B); we name AP+ the electrically coupled T-tubules and AP− the failing elements. Failing T-tubules are never observed in WT cardiomyocytes. In Fig. 5C representative Ca^{2+} traces correspondent to AP+ and AP− T-tubules are overlapped showing a prolonged Ca^{2+} rise in AP−. Local Ca^{2+} transient time-to-peak (TTP) is prolonged in cTnT Δ160E cardiomyocytes compared to WT (49.7 ± 1.9 ms vs. 43.2 ± 1.0; $p < 0.001$). Differences in AP duration cannot account for the delay of Ca^{2+} transients found in cTnT Δ160E; in fact, the 50% AP duration is (14.1 ± 1.0) ms in WT and (14.7 ± 1.5) ms in cTnT Δ160E. By separately analysing the two populations of T-tubules, we find a significant delay of TTP both in AP+ and AP− elements (Fig. 5D). However, in AP+ the delay is modest while AP− tubules show a much larger delay.

3.6. Ca^{2+} release variability in cTnT Δ160E mouse model

By studying Ca^{2+} release at multiple sites within the same cell, we observe some variability both in time (beat-to-beat at the same site) and in space (among different sites). In Fig. 6A, we superimposed three subsequent Ca^{2+} traces recorded in three different T-tubules of a WT and cTnT Δ160E myocyte. Even in WT cardiomyocytes, T-tubules display a non-negligible variability of the Ca^{2+} release. However, such variability is remarkably more prominent in the cTnT Δ160E cardiomyocytes. A coefficient of variability (CV) is calculated as σ/μ, where σ is the standard deviation and μ is the mean. CV of Ca^{2+} release is calculated based on time (beat-to-beat CV) and space (spatial CV) and the correspondent graphs are reported in Fig. 6B–C. Both populations of T-tubules (AP+ and AP−) display a strongly increased variability compared to WT highlighting that such variability is not directly related to electrical defects of T-tubules, but rather it could be attributed to alterations of other E–C coupling players. Fig. 6D shows WT (dark grey) and cTnT Δ160E cells (blue) mean traces obtained averaging all local Ca^{2+} releases acquired in the two groups. As highlighted by the two arrows, the averaged cTnT Δ160E trace shows a delayed TTP, the extent of which (~15 ms) is comparable with that found by measuring global Ca^{2+} transients in single cells (Fig. 3B).

3.7. Ca^{2+} sparks frequency in cTnT Δ160E mouse model

The sensitivity of the RAMP imaging system is high enough to detect Ca^{2+} sparks, i.e. Ca^{2+} release events occurring at single calcium release units [29], during a regularly paced sequence of Ca^{2+} transients. We observe spontaneous Ca^{2+} sparks at any time during the Ca^{2+} cycle, either in systole or in diastole (Fig. 6E). Any detectable variation of local membrane potential is observed in correspondence with the sparks, as previously described in other disease models [5]. In WT, we find a significantly higher frequency of Ca^{2+} sparks (fs) during systole. The frequency of Ca^{2+} sparks detected in cTnT Δ160E cardiomyocytes is significantly increased during diastole as compared to WT cells while systolic Ca^{2+} sparks are not augmented. No statistical difference of sparks frequency is found between AP− and AP+ T-tubules.

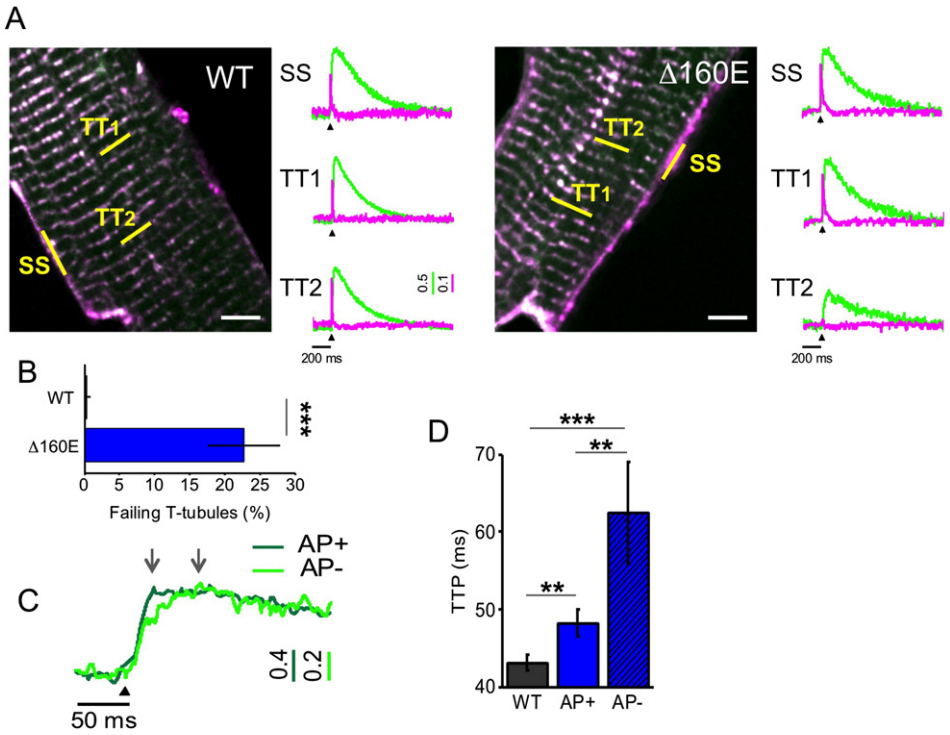

Fig. 5. Defects of T-tubules electrical activity and local calcium release in cTnT Δ160E. (A) Left: two-photon fluorescence (TPF) image of a stained cTnT Δ160E ventricular myocyte: sarcolemma in magenta (di-4-AN(F)EPPTEA) and $[Ca^{2+}]_i$ in green (GFP-certified Fluoforte). Scale bar in white: 5 μm. Right: representative normalized fluorescence traces ($\Delta F/F_0$) of SS and two T-tubules (TTi) recorded in WT and cTnT Δ160E cardiomyocyte (average of ten subsequent trials). Membrane potential in magenta, $[Ca^{2+}]_i$ in green. AP elicited at 200 ms (black arrowheads). (B) Columns showing the percentage of electrically failing T-tubules in WT and cTnT Δ160E myocytes. Data from 101 WT and 66 cTnT Δ160E T-tubules (Students's t-test ***$p < 0.001$). (C) Superposition of fluorescence Ca^{2+} traces ($\Delta F/F_0$) of electrically coupled (AP+, dark green) and uncoupled (AP−, green) T-tubules reported in (A). The two grey arrows pinpoint Ca^{2+} transients TTP of the traces. Electrical trigger provided at 200 ms (black arrowhead). (D) Columns showing time-to-peak (TTP) mean values of Ca^{2+} release measured in cTnT Δ160E cells with respect to WT. Ca^{2+} transient kinetics is reported by separately analysing the two populations of T-tubules (AP+ and AP−). Data reported as mean ± SEM from 101 WT T-tubules, 65 AP+, and 15 AP− (n = 28 WT and 17 cTnT Δ160E; N = 10 WT and 7 cTnT Δ160E). Students's t-test **$p < 0.01$, ***$p < 0.001$.

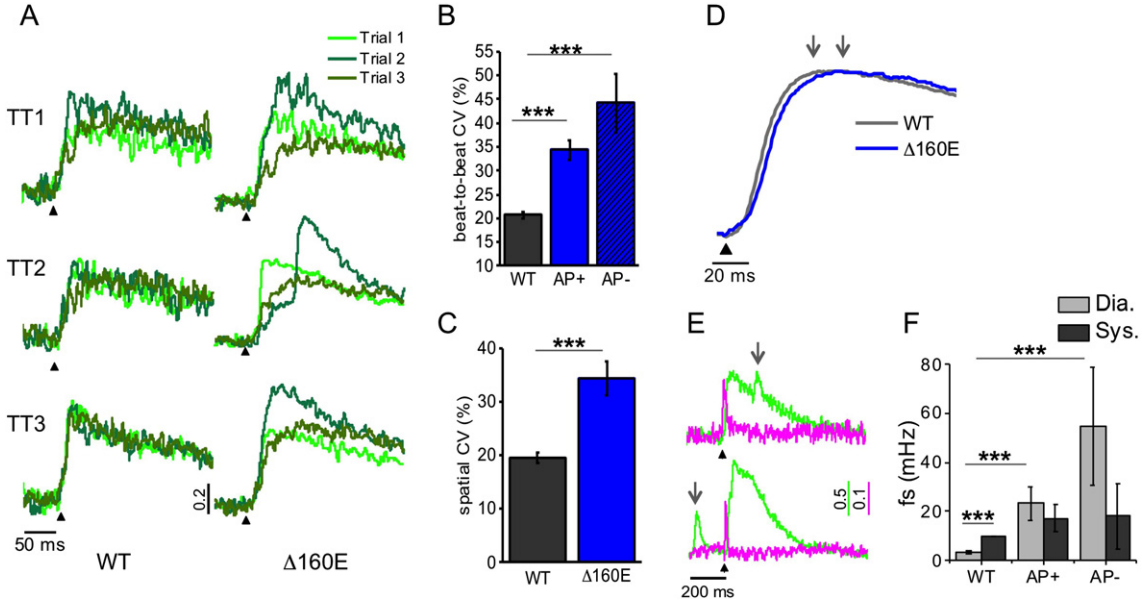

Fig. 6. Variability of Ca^{2+} release and Ca^{2+} sparks. (A) Superposition of three subsequent Ca^{2+} transients recorded in three different T-tubules (TTi) of WT and cTnT Δ160E cardiomyocytes. (B-C) Graphs showing Ca^{2+} release coefficient of variability (CV) calculated at TTP based on time (beat-to-beat CV) and on space (spatial CV). Data from 28 WT cells and 17 cTnT Δ160E myocytes. AP+ and AP− of cTnT Δ160E are separately analysed in beat-to-beat CV. (D) Average of Ca^{2+} transients recorded from 28 WT (grey) and 17 cTnT Δ160E (blue) cardiomyocytes. The two arrows pinpoint the TTP in the transients. (E) Two representative traces of Ca^{2+} sparks recorded in cTnT Δ160E cells either in diastole and systole, grey arrows pinpointing the Ca^{2+} spark occurrence. (F) Columns showing Ca^{2+} spontaneous sparks frequency (fs) recorded in 101 TTs of WT cells, 65 AP+ and 15 AP− of cTnT Δ160E myocytes (Data shown as mean ± SEM, N = 10 WT and 7 cTnT Δ160E). Ca^{2+} sparks recorded during Ca^{2+} transient (CaT95) are considered systolic, while the others are diastolic. Student's t-test applied; **$p < 0.01$ ***$p < 0.001$.

4. Discussion

In the present study, we examine the cTnT Δ160E mutation associated with a severe form of HCM in patients [17,18]. Mice employed are 6–8 months old, reflecting early stages of the disease [20]. Although the causing mutation exerts a direct effect on the sarcomere (i.e. increased sarcomeric Ca^{2+} sensitivity and increased ATPase activity/force, likely related to faster cross-bridge detachment [19]), it also determines a profound dysregulation of Ca^{2+} homeostasis at the cellular level [20]. Specifically, a previous work on cTnT Δ160E cardiomyocytes has demonstrated significant decreases in the peak rate and percent amplitude of unloaded shortening as well as a decrease in the peak rate of relaxation [28]. Consistent alterations were found in the peak rates and times of the rise and decline of global Ca^{2+} transients, with reductions in SR Ca^{2+} load and SERCA function [28]. According to those results, both sarcomere changes (e.g. increased Ca^{2+} sensitivity) and E–C coupling alterations (e.g. reduced SERCA activity) may contribute to the slower relaxation in cTnT Δ160E cardiomyocytes. These previous studies, however, do not fully unveil the relationship between E–C coupling defects and contractile dysfunction and, particularly, they do not provide any mechanistic explanation for the markedly delayed Ca^{2+} rise and slow force development in cTnT Δ160E myocardium.

Here, we perform mechanical measurements on cTnT Δ160E trabeculae, in which twitch tension can be studied in nearly physiological conditions (e.g. isometric load, high stimulation frequencies) and we implement RAMP microscopy to assess simultaneously the electrical activity of T-tubules and the correspondent local Ca^{2+} release in multiple sites of an isolated cell.

Before discussing the role of TATS remodelling in the prolongation of contraction kinetics of cTnT Δ160E myocardium we can exclude that it is related to changes in myosin isoform expression. Indeed both WT and cTnT Δ160E mice express only α-MHC in their ventricles (Fig. 1D).

The first remarkable observation is that more than 20% of T-tubules fail in propagating AP and also exhibit a significant delay of local Ca^{2+} release. This finding can be directly linked to the slower force generation found in cTnT Δ160E trabeculae. Compromised T-tubular system has been recently related to analogous mechanical alterations in acutely detubulated trabeculae [3]. In the cTnT Δ160E, however, the extent of structural alterations of the tubular system (investigated here by confocal analysis) can hardly account for the remarkable contractile impairment measured in trabeculae, making a detailed functional investigation essential. In fact, we previously demonstrated that: i) the mere presence of a T-tubule does not ensure its electrical function [6]; ii) even electrically coupled tubules can be associated with impaired Ca^{2+} transients in a pathological context [5]. This is confirmed in cTnT Δ160E cardiomyocytes, where the Ca^{2+} rise is delayed as compared to WT, both at propagating (AP+) and non-propagating (AP−) tubules. However, the delay of local Ca^{2+} transient TTP is modest in AP+ tubules (~5 ms) and much longer in AP− (~19 ms), indicating a major contribution of AP− to the prolongation of global Ca^{2+} rise. Molecular mechanisms underlying delayed Ca^{2+} rise in AP+ may comprise dyadic ultrastructural alterations (e.g. DHPR-RyR2 uncoupling) as well as functional changes of T-tubular membrane channels or alterations of RyR2 gating (discussed below). The additional delay in AP− areas is due to the slow Ca^{2+}-induced Ca^{2+}-release propagation form neighbouring AP+ tubules, as described in previous works [3,5]. The co-existence of sarcomeres with reduced and delayed Ca^{2+} activation (corresponding to AP−) in series with sarcomeres with fast and higher Ca^{2+} activation may itself decrease the uniformity of cardiomyocyte contraction, thus reducing developed force and slowing the kinetics of force development.

Changes of the spatial variability of Ca^{2+} release (studied by comparing Ca^{2+} transients occurring simultaneously at different T-tubular sites within cells) may additionally promote the global prolongation of Ca^{2+} rise found in cTnT Δ160E cells and enhance non-homogeneous myofilament activation. Indeed, a remarkably increased spatio-temporal variability of local Ca^{2+} transient TTP is observed in cTnT Δ160E cells with respect to WT.

In addition to slower kinetics of contraction, cTnT Δ160E trabeculae show increased amplitude of premature contractions (i.e. faster mechanical restitution) and depressed post-rest potentiation with spontaneous activity during stimulation pauses. Interestingly, faster mechanical restitution occurs despite a slower SR Ca^{2+} re-uptake, as described in previous studies [28]. These results may be related with an increased RyR2 open probability, which determines shorter SR refractoriness and promotes SR Ca^{2+} load depletion through diastolic Ca^{2+} leak. Indeed, cTnT Δ160E myocytes exhibit an increased frequency of Ca^{2+} sparks in diastole compared to WT. The higher diastolic intracellular Ca^{2+} levels observed in cTnT Δ160E cardiomyocytes compared to WT may be an additional evidence of increased diastolic SR Ca^{2+} leak. Multiple changes occurring in cTnT Δ160E cardiomyocytes [20], including post-translational modifications affecting RyR function (e.g. variations of phosphorylation levels), may be the cause of the observed increased diastolic Ca^{2+} sparks frequency, that occurs in cTnT Δ160E despite a reduced SR Ca^{2+} content. A different hypothesis is that higher diastolic Ca^{2+} results from a slower Ca^{2+} dissociation from the sarcomeres due to the mutation-related increased myofilament Ca^{2+} sensitivity. Higher cytosolic Ca^{2+} coming from the sarcomeres may secondarily promote aberrant RyR2 activation, thus representing the cause rather than the consequence of increased SR spontaneous leakage. These hypotheses could co-exist and do not exclude the contribution of additional pathophysiological mechanisms, e.g. reduced forward mode NCX activity contributing to slower cytosolic Ca^{2+} removal and thus higher diastolic Ca^{2+}. The reduced (diastolic) SR Ca^{2+} content observed in cTnT Δ160E could antagonize the effects of increased cytosolic Ca^{2+} levels and this complex scenario may also be complicated by local differences in SR load and RyR2 refractoriness, related to the spatial variability of Ca^{2+} release and the delayed Ca^{2+} rise at failing (AP−) tubules in cTnT Δ160E cardiomyocytes. Further studies are needed to clarify these aspects of local RyR2 gating control. Importantly, systolic Ca^{2+} sparks frequency is similar in cTnT Δ160E cardiomyocytes compared to WT, suggesting no major changes of RyR2 gating at low SR Ca^{2+} load during systole.

From the arrhythmogenic perspective, the increased rate of diastolic Ca^{2+} sparks in cTnT Δ160E myocardium may be the cause of spontaneous contractions observed in mutant trabeculae. Indeed, multiple sparks occurring within a cell may lead to calcium waves, delayed after depolarizations and premature spontaneous action potentials, which would propagate to the whole trabecula, generating a spontaneous premature contraction. Our RAMP experimental conditions, featuring low inotropic levels to minimize cell movement and to isolate single events, do not allow propagation of cell-spanning Ca^{2+} waves arising from sparks. Although we could not directly demonstrate the link between local Ca^{2+} sparks with spontaneous contractile activity, they are likely to play a significant role in this pathology.

The spatio-temporal relationship between T-tubular electrical activity and Ca^{2+} release was recently investigated using RAMP microscopy in HF [3,5,6]. Similarly to cTnT Δ160E, some HF T-tubules fail in propagating AP, producing dramatic consequences on Ca^{2+} synchrony and kinetics. The percentage of failing sites in cTnT Δ160E is four times higher than that observed in HF. On the other hand, HCM cardiomyocytes do not show spontaneous depolarizations of T-tubules or voltage-associated sparks (which are observed in HF). This result suggests that T-tubule functional alterations can be widely diverse, producing different consequences, probably due to specific biochemical signals triggered by the two different pathologies. In our HCM mouse model, a severe dysfunction of the T-tubules occurs in the absence of a massive structural T-tubular remodelling, as seen in secondary heart diseases such as HF. In fact, HCM is a genetic disease that impacts directly on the sarcomere and, therefore, contractile dysfunction often precedes any other pathological modification. How sarcomere mutations cause

impairments of T-tubular function in HCM remains, however, to be investigated.

In conclusion, we demonstrate that, even in the presence of mild structural alterations, T-tubules function can be severely compromised in HCM. Some mechanical alterations of cTnT Δ160E myocardium, i.e. slower force development can be attributed directly to electrical defects of T-tubules and correspondent local Ca^{2+} anomalies. The development of non-invasive ultrafast imaging modalities [30] for probing multi-sited and fast phenomena opens new possibilities to disclose cellular mechanistic insights capable of explaining pathological phenotypes.

Acknowledgements

The research leading to these results received funding from the European Union Seventh Framework Programme (FP7/2007–2013) under Grant Agreements 241577, 241526, and 284464. This research project was also supported by National Institutes of Health (NIH Grant: R01 EB001963), by the Italian Ministry for Education, University and Research in the framework of the Flagship Project NANOMAX, by the Italian Ministry of Health (WFR GR-2011-02350583) and by Telethon–Italy (GGP13162).

References

[1] C. Ferrantini, C. Crocini, R. Coppini, F. Vanzi, C. Tesi, E. Cerbai, et al., The transverse-axial tubular system of cardiomyocytes, Cell. Mol. Life Sci. 70 (2013) 4695–4710.
[2] F. Brette, S. Despa, D.M. Bers, C.H. Orchard, Spatiotemporal characteristics of SR Ca(2+) uptake and release in detubulated rat ventricular myocytes, J. Mol. Cell. Cardiol. 39 (2005) 804–812.
[3] C. Ferrantini, R. Coppini, L. Sacconi, B. Tosi, M.L. Zhang, G.L. Wang, et al., Impact of detubulation on force and kinetics of cardiac muscle contraction, J. Gen. Physiol. 143 (2014) 783–797.
[4] L.S. Song, E.A. Sobie, S. McCulle, W.J. Lederer, C.W. Balke, H. Cheng, Orphaned ryanodine receptors in the failing heart, Proc. Natl. Acad. Sci. U. S. A. 103 (2006) 4305–4310.
[5] C. Crocini, R. Coppini, C. Ferrantini, P. Yan, L.M. Loew, C. Tesi, et al., Defects in T-tubular electrical activity underlie local alterations of calcium release in heart failure, Proc. Natl. Acad. Sci. U. S. A. 111 (2014) 15196–15201.
[6] L. Sacconi, C. Ferrantini, J. Lotti, R. Coppini, P. Yan, L.M. Loew, et al., Action potential propagation in transverse-axial tubular system is impaired in heart failure, Proc. Natl. Acad. Sci. U. S. A. 109 (2012) 5815–5819.
[7] R.R. Kaprielian, S. Stevenson, S.M. Rothery, M.J. Cullen, N.J. Severs, Distinct patterns of dystrophin organization in myocyte sarcolemma and transverse tubules of normal and diseased human myocardium, Circulation 101 (2000) 2586–2594.
[8] S. Kostin, D. Scholz, T. Shimada, Y. Maeno, H. Mollnau, S. Hein, et al., The internal and external protein scaffold of the T-tubular system in cardiomyocytes, Cell Tissue Res. 294 (1998) 449–460.
[9] B.J. Maron, V.J. Ferrans, W.C. Roberts, Ultrastructural features of degenerated cardiac muscle cells in patients with cardiac hypertrophy, Am. J. Pathol. 79 (1975) 387–434.
[10] J. Schaper, R. Froede, S. Hein, A. Buck, H. Hashizume, B. Speiser, et al., Impairment of the myocardial ultrastructure and changes of the cytoskeleton in dilated cardiomyopathy, Circulation 83 (1991) 504–514.
[11] A.R. Lyon, K.T. MacLeod, Y. Zhang, E. Garcia, G.K. Kanda, M.J. Lab, et al., Loss of T-tubules and other changes to surface topography in ventricular myocytes from failing human and rat heart, Proc. Natl. Acad. Sci. U. S. A. 106 (2009) 6854–6859.
[12] T. Force, R.O. Bonow, S.R. Houser, R.J. Solaro, R.E. Hershberger, B. Adhikari, et al., Research priorities in hypertrophic cardiomyopathy: report of a Working Group of the National Heart, Lung, and Blood Institute, Circulation 122 (2010) 1130–1133.
[13] C.Y. Ho, Hypertrophic cardiomyopathy, Heart Fail. Clin. 6 (2010) 141–159.
[14] C. Poggesi, C.Y. Ho, Muscle dysfunction in hypertrophic cardiomyopathy: what is needed to move to translation? J. Muscle Res. Cell Motil. 35 (2014) 37–45.
[15] R. Coppini, C. Ferrantini, L. Yao, P. Fan, M. Del Lungo, F. Stillitano, et al., Late sodium current inhibition reverses electromechanical dysfunction in human hypertrophic cardiomyopathy, Circulation 127 (2013) 575–584.
[16] A.M. Varnava, P.M. Elliott, C. Baboonian, F. Davison, M.J. Davies, W.J. McKenna, Hypertrophic cardiomyopathy: histopathological features of sudden death in cardiac troponin T disease, Circulation 104 (2001) 1380–1384.
[17] F. Pasquale, P. Syrris, J.P. Kaski, J. Mogensen, W.J. McKenna, P. Elliott, Long-term outcomes in hypertrophic cardiomyopathy caused by mutations in the cardiac troponin T gene, Circ. Cardiovasc. Genet. 5 (2012) 10–17.
[18] H. Watkins, W.J. McKenna, L. Thierfelder, H.J. Suk, R. Anan, A. O'Donoghue, et al., Mutations in the genes for cardiac troponin T and alpha-tropomyosin in hypertrophic cardiomyopathy, N. Engl. J. Med. 332 (1995) 1058–1064.
[19] M. Chandra, M.L. Tschirgi, J.C. Tardiff, Increase in tension-dependent ATP consumption induced by cardiac troponin T mutation, Am. J. Physiol. Heart Circ. Physiol. 289 (2005) H2112–H2119.
[20] R.K. Moore, L.T. Grinspan, J. Jimenez, P.J. Guinto, B. Ertz-Berger, J.C. Tardiff, HCM-linked 160E cardiac troponin T mutation causes unique progressive structural and molecular ventricular remodeling in transgenic mice, J. Mol. Cell. Cardiol. 58 (2013) 188–198.
[21] P.P. de Tombe, H.E. ter Keurs, Force and velocity of sarcomere shortening in trabeculae from rat heart. Effects of temperature, Circ. Res. 66 (1990) 1239–1254.
[22] A. Belus, N. Piroddi, B. Scellini, C. Tesi, G. D'Amati, F. Girolami, et al., The familial hypertrophic cardiomyopathy-associated myosin mutation R403Q accelerates tension generation and relaxation of human cardiac myofibrils, J. Physiol. 586 (2008) 3639–3644.
[23] P.J. Reiser, W.O. Kline, Electrophoretic separation and quantitation of cardiac myosin heavy chain isoforms in eight mammalian species, Am. J. Physiol. 274 (1998) H1048–H1053.
[24] L. Toniolo, L. Maccatrozzo, M. Patruno, F. Caliaro, F. Mascarello, C. Reggiani, Expression of eight distinct MHC isoforms in bovine striated muscles: evidence for MHC-2B presence only in extraocular muscles, J. Exp. Biol. 208 (2005) 4243–4253.
[25] R.J. Talmadge, R.R. Roy, Electrophoretic separation of rat skeletal muscle myosin heavy-chain isoforms, J. Appl. Physiol. 75 (1993) 2337–2340.
[26] P. Yan, C.D. Acker, W.L. Zhou, P. Lee, C. Bollensdorff, A. Negrean, et al., Palette of fluorinated voltage-sensitive hemicyanine dyes, Proc. Natl. Acad. Sci. U. S. A. 109 (2012) 20443–20448.
[27] A. Guo, L.S. Song, AutoTT: automated detection and analysis of T-tubule architecture in cardiomyocytes, Biophys. J. 106 (2014) 2729–2736.
[28] T.E. Haim, C. Dowell, T. Diamanti, J. Scheuer, J.C. Tardiff, Independent FHC-related cardiac troponin T mutations exhibit specific alterations in myocellular contractility and calcium kinetics, J. Mol. Cell. Cardiol. 42 (2007) 1098–1110.
[29] H. Cheng, W.J. Lederer, M.B. Cannell, Calcium sparks: elementary events underlying excitation-contraction coupling in heart muscle, Science 262 (1993) 740–744.
[30] C. Crocini, R. Coppini, C. Ferrantini, F.S. Pavone, L. Sacconi, Functional cardiac imaging by random access microscopy, Front. Physiol. 5 (2014) 403.